Li, Dayan; Kelly, Damien P.; Sheridan, John T. :

Experimental exploration of the correlation coefficient of static speckles in Fresnel configuration

Zuerst erschienen in:
Dimensional optical metrology and inspection for practical applications. - Bellingham, Wash. : SPIE, 2011. - ISBN 978-0-8194-8748-3. - 813310, insges. 13 S.
(Proceedings of SPIE ; 8133)
DOI: 10.1117/12.895541

Experimental exploration of the correlation coefficient of static speckles in Fresnel configuration

Dayan Li[a], Damien P. Kelly[b], John T. Sheridan*[a]
[a]UCD Communications and Optoelectronic Research Centre, SFI-Strategic Research Cluster in Solar Energy Conversion, University College Dublin, Belfield, Dublin 4, Ireland.
[b]Institut für Mikro- und Nanotechnologien, Macro-Nano, Fachgebiet Optik Design, Technische Universität Ilmenau, Postfach 100565, 98684 Ilmenau, Germany.

ABSTRACT

Quasi-monochromatic light reflected from an optically rough surface produces a complicated 3D speckle field. This speckle field is often described using a correlation function from which the 3D speckle properties can be examined. The derivation of the correlation function is based on a physical model where several critical assumptions about the input and output fields in the model are made. However, experimental works verifying this correlation function are rare and sometimes produce inconsistent results. In this paper, we examine some practical issues encountered when experimentally measuring this correlation function, including: The realization of the ensemble average between speckle fields at two point positions; and, The pixel integrating effect of the recording camera and the implications this has for the statistics of the measured speckle field. Following verification of the correlation function and examining the speckle decorrelation properties in 3D space, two practical applications are proposed, one is the aligning of the system optical axis with the camera center and the other is the measurement of the out-of-plane displacement of an object surface. Simulation and experimental results that support our analysis are presented.

Keywords: speckle correlation coefficients, ensemble average, pixel integrating effect, longitudinal decorrelation, alignment algorithm, out-of-plane displacement measurement

1. INTRODUCTION

A 3D speckle field is produced when an optically rough surface is illuminated by coherent laser light. Statistical properties of the resultant speckle fields are usually examined by studying the space-time cross-correlation function in the observation plane that is perpendicular to the optical axis. In 1990 Leushacke and Kirchner [1] examined the 3D structure of static speckle under plane wave illumination. Li and Chiang [2] also investigated 3D speckle and measured the lateral and on-axis longitudinal speckle size, respectively by examining the diffraction halos and the Young's fringes of the specklegrams. Later, the 3D space-time cross-correlation function for free space geometry under Gaussian beam illumination was presented by Yoshimura and Iwamoto [3]. Theoretically the speckle correlation between fields at any two different point positions in the free-space Fresnel regime can be found using the analytic expressions presented in [1] and [3]. The analysis in these manuscripts has been extended to include other paraxial optical systems and soft Gaussian apertures using *ABCD*-matrix theory [4, 5]. A generalized Yamaguchi correlation factor was also derived for the paraxial systems with a hard limiting aperture [6, 7]. Basically, all the derivations of the analytic correlation function in [1-7] are based on the well known physical model for fully developed speckle [8], in which several critical assumptions have been made to simplify the theoretical analysis: (i) The autocorrelation of the field at the diffuser surface (object plane) is a delta function; (ii) The surface roughness is optically rough producing phase variations uniformly distributed over $[0 - 2\pi]$; and (iii) The real and the imaginary parts of the field at the diffuser surface are uncorrelated. With these assumptions speckle fields in the observation plane obey a complex Gaussian random process [8]. It is important to justify these assumptions, hence experimental verification of the analytic correlation function is of great theoretical interest.

*john.sheridan@ucd.ie; phone 353 1 716-1927; fax 353 1 283 0921; eleceng.ucd.ie/~jsheridan/

However, as noted in [2], no consistent experimental results on the longitudinal speckle size were reported when photosensitive films were being used as the recording materials [9, 10]. Digital cameras (CCDs) are now widely used to record speckle patterns, which simplifies the experimental procedure for testing the validity of these approximations. Nevertheless experimental investigations of the longitudinal speckle correlation properties are relatively rare compared with the numerous theoretical derivations that have been developed based on these assumptions [1-3, 7-8, 11-12]. In Ref. [13] the authors present a new theoretical model for the description of speckle fields. The model predicts a series of interesting speckle characteristics (in three different regimes) that are demonstrated experimentally in a follow-up paper [14]. In this model the input field is assumed to be factorized into two well-separated spatial variations: one describes the lateral average speckle size and the other is the lateral size of the illuminating spot in the input plane. The input field is no longer assumed to be delta correlated (in the input plane) as is the case for the model examined in this paper. However, the input field in [13] can be considered as being generated by a delta correlated field which then propagates a specific longitudinal distance z_0 to the input plane. As a result, identical speckle characteristics are predicted by the authors of [13] [in the Van Cittert-Zernike (VCZ) regime], and by us (calculated for the Fresnel regime), when equivalent propagation distances are used, i.e., see Eq. (41) in [13] and Eq. (5) below.

In this paper we experimentally determine this correlation function [Eq. (5) below] and compare it to the predictions of the physical model. We note that performing such a comparison is not straightforward. First, since the camera pixel is not an ideal point-like detector, the integrating effect of the finite size pixel on the statistics of measured speckle intensity needs to be looked at. Therefore we extend the traditional derivation of the correlation function so that it includes the integrating effect of the camera pixel, showing that this effect can be made negligible provided that the ratio of the camera pixel size to the speckle lateral correlation extent is properly controlled [15].

Secondly, the correlation function is mathematically represented by the ensemble average between the intensity values at the two point positions. Theoretically, ensemble average of speckle intensity requires that a large ensemble of temporally ergodic fields has to be generated. In practice this ensemble average can be realized either by time averaging or by spatial averaging, depending on the speckle fields that are assumed to be ergodic in time or in space [16, 17]. To perform time averaging, a large number of intensities for these two specific points have to be measured, where the diffuser used to generate the speckle fields is replaced with a new statistically similar one for each of these measurements. As can be expected, this process is very time-consuming. In spatial averaging, the temporally ergodic speckle fields are approximated by a large number of intensities around the two points. Therefore the measurement process just involves one diffuser. In this paper we present simulated results realized using a time averaging. By comparing the results with those generated using a spatial averaging as presented in [18], we conclude that the two realization methods provide effectively equivalent results for the static free-space speckles. Hence we provide evidence justifying our experimental technique for estimating correlation coefficients using a spatial averaging.

In the experiments, the variations of the speckle intensity statistics caused by the camera pixel are measured. Then we measure the lateral and longitudinal correlation function of speckle, so that the critical assumptions, mentioned above, are experimentally verified. Two practical applications are implied by the experimental study of the speckle correlation function. These applications are both based on extracting quantitive values for the correlation coefficients between two longitudinally displaced speckle patterns. A more detailed description of the experimental measurements and the implied applications can be found in [19].

2. 3D SPECKLE CORRELATION FUNCTION

2.1 Theory

In this section we briefly review the derivation of the 3D speckle correlation function. The free-space optical setup is shown in Fig. 1. A diffuser is placed in the object plane (ξ, η) and illuminated from behind with monochromatic light of wavelength λ. The scattered light propagates to the observation plane (x, y) where the speckle intensity pattern is recorded by a camera, located a distance z_0 from the object plane. Here we restrict our attention to fully developed speckle formed when the surface roughness exceeds the wavelength of the illuminating light and where the surface correlation extent is much smaller than the illuminated area. Based on the critical assumptions mentioned in Section 1

for the fully developed speckle, the normalized correlation function between the speckle intensities at point positions $\boldsymbol{r}$ and $\boldsymbol{r'}$ can be given by the ensemble average as [1-3, 8, 18]

$$\frac{< I(\boldsymbol{r})I(\boldsymbol{r'}) >}{< I(\boldsymbol{r}) >< I(\boldsymbol{r'}) >} = 1 + \left|\mu_{12}(\boldsymbol{r},\boldsymbol{r'})\right|^2 \tag{1}$$

and

$$\left|\mu_{12}(\boldsymbol{r},\boldsymbol{r'})\right|^2 = \left| \frac{\iint \left|E(\boldsymbol{p})\right|^2 \exp\left[ik\left(\left|\boldsymbol{r}-\boldsymbol{p}\right| - \left|\boldsymbol{r'}-\boldsymbol{p}\right|\right)\right] d\xi d\eta}{\iint \left|E(\boldsymbol{p})\right|^2 d\xi d\eta} \right|^2, \tag{2}$$

where $|E(\boldsymbol{p})|$ represents the illuminating wave amplitude (a more detailed derivation of the correlation function can be found in [1, 3, 18]). It can be seen that $|\mu_{12}|^2$ depends on the intensity distribution of the illuminating beam, the shape and size of the illuminating spot on the object and the observation positions ($\boldsymbol{r}$, $\boldsymbol{r'}$) with respect to the origin, O = (0, 0, 0), which is defined by the location of the centre of the illuminating spot. We compare the cases of plane wave and Gaussian beam illuminations by making the appropriate substitutions for $|E(\boldsymbol{p})|$.

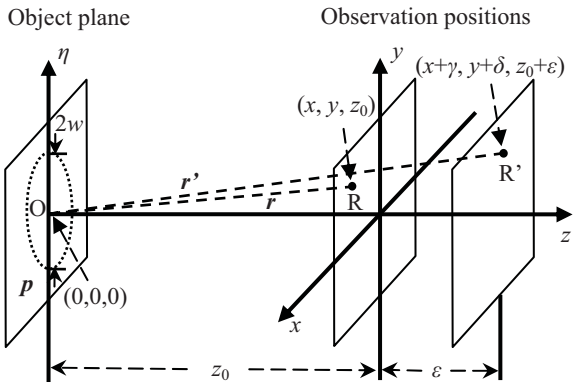

Figure 1. Free space propagation geometry for static speckle formation. The illuminating spot on the diffuse object is circular with diameter $2w$.

For plane wave illumination, $|E(\boldsymbol{p})|$ is constant when $|\boldsymbol{p}| \le w$ and zero otherwise. The expression for $|\mu_{12}|^2$, between field at point positions $\boldsymbol{r} = (x, y, z_0)$ and $\boldsymbol{r'} = (x + \gamma, y + \delta, z_0 + \varepsilon)$, as indicated in Fig. 1, is simplified to [1, 18]

$$\left|\mu_{12}(x,y,z_0;\gamma,\delta,\varepsilon)\right|^2 = \left| 2\sum_{n=0}^{\infty} i^n (2n+1) j_n(u/4) J_{2n+1}(v)/v \right|^2, \tag{3}$$

where $u = -w^2 \varepsilon k / z_0^2$, $v = wk\sqrt{(z_0\gamma - \varepsilon x)^2 + (z_0\delta - \varepsilon y)^2}\,/\,z_0^2$, and $k = 2\pi/\lambda$. j_n are the spherical Bessel functions and J_n are the Bessel function of the first kind.

For Gaussian beam illumination, we define [3, 20]

$$\left|E(\boldsymbol{p})\right| = \left(\frac{w_0}{w}\right)^2 \exp\left(-\frac{\left|\boldsymbol{p}\right|^2}{w^2}\right), \tag{4}$$

where w is the radius at which the beam amplitude drop to $1/e$ of the axial value in the object plane, and w_0 is a constant denoting the beam waist size. The expression for $|\mu_{12}|^2$ is simplified to [3, 18]

$$\left|\mu_{12}(x,y,z_0;\gamma,\delta,\varepsilon)\right|^2 = \frac{1}{1+(\varepsilon/l_z)^2}\exp\left\{-\left(\frac{1}{r_s}\right)^2\left[\left(\frac{\varepsilon}{z_0}x-\gamma\right)^2+\left(\frac{\varepsilon}{z_0}y-\delta\right)^2\right]\right\}, \tag{5}$$

where $l_z = 4z_0(z_0+\varepsilon)/(w^2k)$, and $r_s = 2(z_0+\varepsilon)[1+(\varepsilon/l_z)^2]^{1/2}/(wk)$.

The speckle correlation coefficient for any two points in the 3D space can be determined using Eq. (3) for plane wave illumination and using Eq. (5) for Gaussian beam illumination. For the interpretation of the correlation function, which gives the speckle decorrelation trend, and thus the speckle size, in the 3D space, the readers are referred to [18].

2.2 Pixel integrating effect

In this subsection we explore the impact of intensity spatial integration resulted from the camera pixel on the speckle correlation. For practical measurements, the detected intensity is the spatially integrated intensity over the finite area of a camera element, which differs from the ideal case of point-like intensity sampling assumed in the theoretical derivation. Considering a camera with finite square pixels, the measured intensity I_α at a single pixel is defined by [8]

$$I_a = \frac{1}{A_D^2}\int\!\!\int_{-\infty}^{\infty} D_a(x,y)I(x,y)dxdy, \tag{6}$$

where A_D denotes pixel size of camera, $I(x, y)$ is the ideal point-like speckle intensity incident at the camera detecting surface, and $D_a(x, y)$ is the pixel aperture function representing the distribution of the camera's photosensitivity over pixel active area.

The second moment of I_α is given by

$$< I_{a1}I_{a2} > = \frac{1}{A_D^4}\int\!\!\int_{-\infty}^{\infty}\int\!\!\int_{-\infty}^{\infty} D_{a1}(x_1,y_1)D_{a2}(x_2,y_2) < I(x_1,y_1)I(x_2,y_2) > dx_1dy_1dx_2dy_2, \tag{7}$$

in which the orders of ensemble average and integration have been interchanged. Using Eq. (1) and noting that $<I_a> = <I>$, which indicates that the mean of the detected intensity is identical with the true mean of the speckle pattern, Eq. (7) can be rewritten as [8]

$$M^{-1} = \frac{< I_{a1}I_{a2} >}{< I_{a1} >< I_{a2} >} - 1$$

$$= \frac{1}{A_D^4}\int\!\!\int_{-\infty}^{\infty}\int\!\!\int_{-\infty}^{\infty} D_{a1}(x_1,y_1)D_{a2}(x_2,y_2)\left|\mu_{12}(x_1,y_1,z_1;x_2,y_2,z_2)\right|^2 dx_1dy_1dx_2dy_2, \tag{8}$$

where we have define M^{-1} as the normalized correlation coefficient for the spatially integrated speckle intensity, and the expression $|\mu_{12}(x_1, y_1, z_1; x_2, y_2, z_2)|^2$ can be found from Eq. (3) (for plane wave illumination) or Eq. (5) (for Gaussian beam illumination), by substituting for the coordinate difference with the corresponding Cartesian coordinate. It can be seen from Eq. (8) that M^{-1} is determined by the pixel aperture function of the camera and $|\mu_{12}(x_1, y_1, z_1; x_2, y_2, z_2)|^2$. Once the two functions have been found, M^{-1} for any two pixels in the 3D space can be determined. M^{-1} is therefore calculated using the corresponding $|\mu_{12}(x_1, y_1, z_1; x_2, y_2, z_2)|^2$ integrating over an area that is limited by the pixel aperture function.

To study the statistics of the integrated speckle intensity, we examine M^{-1} at a single pixel in the observation plane $z = z_0$, which is the auto-correlation of the integrated speckle intensity in this plane. Thus for Eq. (8) we have $D_{a1}(x_1, y_1) = D_a(x_1, y_1)$, $D_{a2}(x_2, y_2) = D_a(x_2, y_2)$, and $z_1 = z_2 = z_0$. Using the coordinate difference $\gamma = x_2\text{-}x_1$ and $\delta = y_2\text{-}y_1$, the auto-correlation of the integrated speckle intensity is given by

$$M_{auto}^{-1} = \frac{1}{A_D^4}\int\int_{-\infty}^{\infty} K_D(\gamma,\delta)\left|\mu_{12}(x_1,y_1,z_0;\gamma,\delta,0)\right|^2 d\gamma d\delta\,, \tag{9}$$

where

$$K_D(\gamma,\delta) = \int\int_{-\infty}^{\infty} D_a(x_1,y_1)D_a(x_1+\gamma,y_1+\delta)dx_1dy_1\,. \tag{10}$$

We note from Eq. (3) and (5) that $|\mu_{12}(x_1, y_1, z_0; \gamma, \delta, 0)|^2$ in the $z = z_0$ plane is independent of position coordinates (x_1, y_1) but is a function of the coordinate difference (γ, δ). Therefore, as expected, the auto-correlation of the camera captured speckle intensity M^1_{auto} also only depends on the coordinate difference (γ, δ), while has nothing to do with the position coordinates (x, y). As a result, the integrated intensity at each camera pixel is governed by the same Probability Density Function (PDF), which can be approximated by the Gamma distribution as (see Section 4.6 from Page 94 in [8]) [15]

$$P(I_\alpha) = \frac{1}{\Gamma(M_{auto})}\left(\frac{M_{auto}}{<I_\alpha>}\right)^{M_{auto}} I_\alpha^{M_{auto}-1}\exp\left(-\frac{M_{auto}I_\alpha}{<I_\alpha>}\right), \tag{11}$$

where M_{auto} is the inverse of M^1_{auto} and $\Gamma(M_{\text{auto}})$ is a Gamma function with argument M_{auto} [21].

In order to see the transformation of the statistics of speckle intensity before and after camera recording, we consider a specific case in which the camera pixel aperture function is square in shape having uniform response, and is defined by the rectangle function as

$$D_a(x,y) = \begin{cases} 1, & -\frac{A_D}{2} \le x \,\&\&\, y \le \frac{A_D}{2} \\ 0, & otherwise \end{cases}. \tag{12}$$

When the speckle patterns are generated under Gaussian beam illumination, from Eq. (5) with ε=0, we have

$$\left|\mu_{12}(x_1,y_1,z_0;\gamma,\delta,0)\right|^2 = \exp\left(-\frac{\gamma^2+\delta^2}{A_C^2}\right), \tag{13}$$

where $A_C = z_0\lambda/(\pi w)$ is the correlation extent of the speckle pattern incident on the camera, which quantifies the average lateral speckle size in this specific plane. Substituting Eq. (12) and (13) into Eq. (9) M^1_{auto} becomes

$$M_{auto}^{-1} = \frac{A_C^2}{A_D^4}\exp\left(-\frac{2A_D^2}{A_C^2}\right)\left[A_C + \exp\left(\frac{A_D^2}{A_C^2}\right)\left[-A_C + A_D\sqrt{\pi}\,\mathrm{erf}\left(\frac{A_D}{A_C}\right)\right]\right]^2, \tag{14}$$

where erf(x) is the standard Error Function [21]. For plane wave illumination, M^1_{auto} can not be obtained the closed-form expression. However, using the same method as for the Gaussian beam illumination, numerical result of M^1_{auto} for plane wave illumination is achievable. In Fig. 2, the results for M^1_{auto} in these two cases are numerically plotted as a function of A_D/A_C, the ratio of the pixel size (A_D) to the correlation extent (A_C) of the speckle pattern. Note that $A_C = z_0\lambda/(2\pi w)$ for the plane wave illumination case.

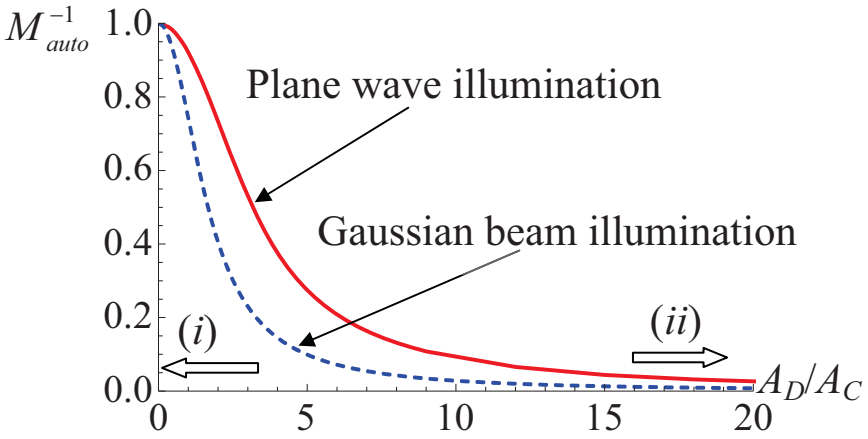

Figure 2. Auto-correlation of the integrated intensity as a function of the ratio of A_D to A_C. Curves are obtained when A_C varies while A_D is fixed at 7.4 μm. Limiting cases: (*i*) $A_D/A_C \ll 1$ and (*ii*) $A_D/A_C \gg 1$

From Fig. 2 we can see that, as expected, the two limiting cases corresponding to (i) $A_D/A_C \ll 1$, point-like detection; and (ii) $A_D/A_C \gg 1$, a greatly extended aperture detection, result in M^{-1}_{auto} values of 1 and 0, respectively. For point-like detection, the PDF of the measured speckle intensity follows exactly the negative exponential distribution, i.e., see Eq. (11) when $M^{-1}_{auto}=1$, which is the theoretical PDF for fully developed speckle. As the ratio A_D/A_C increases, the PDF of the measured intensity changes to a Gamma distribution with argument M_{auto}. Therefore, M^{-1}_{auto} can be interpreted as the average number of speckles influencing the measurements [8], which is a function of the ratio of the pixel size (A_D) to the correlation extent (A_C) of the speckle pattern. When $A_D/A_C \ll 1$, M^{-1}_{auto} converges to unity as A_D/A_C decreases, indicating that no matter how small the measurement aperture is, a minimum of one speckle will influence the result. On the other hand, when $A_D/A_C \gg 1$, M^{-1}_{auto} then has a very low (near to zero) constant value for a large range of A_D/A_C, indicating that in this case, the change of the statistics of the speckle intensity, i.e., the correlation extent (A_C), is not detected because the pixel size A_D is too large compared to the average speckle size.

These results predict that during experiments, the average lateral speckle size on the camera surface should be much larger than the camera pixel size. It can be inferred from Fig. 2 that the integrating effect of the camera decreases in proportion to A_D/A_C. Knowing of A_D/A_C, the first order statistics of the captured speckle intensity can be analysed using Eq. (11), the experimental verification of this is presented in Section 4.

3. ENSEMBLE AVERAGE OF SPECKLE

As stated in Eq. (1), the correlation function of the speckle intensity is represented by the ensemble average between the speckle fields at two point positions. To realize the ensemble average, the speckle intensities at the positions of interest are recorded for a series of different but statistically similar diffusers. This is the basic principle of ensemble average realized using a time averaging. However, for the static speckle fields, the intensities in the observation plane are also approximately similar over a spatial area about the positions of interest. Hence, the ensemble average of static speckle can also be determined using a single recording of an area speckle pattern. In this case, the area intensity at points around the position of interest is used to approximate the temporally ergodic fields. This is the basic principle of ensemble average realized by a spatial averaging. In [18], we have described a simulation technique to generate speckle patterns in the observation plane. The speckle correlation coefficients computed from these patterns using spatial averaging are presented in [18]. Here we simulate the speckle intensities for the Gaussian beam illumination case and compute the resulting correlation function using a time averaging. We will see that the time averaging provides identical results in the static speckle correlation as the spatial averaging.

3.1 Simulating temporally ergodic speckle intensities

For our numerical simulation, the temporally ergodic speckle intensities are generated as follows: A square matrix of dimension $N \times N$, is used to describe the input field immediately in front of the diffuser, i.e., the object plane in Fig. 1.

Within this square matrix, a sub-array of "circular diameter" C samples is used to model the finite extent of the illuminating field on the object surface. This sample number C is defined to be $C = 2w/\Delta\xi$, where $\Delta\xi$ is the sampling period in the object plane. To proceed numerically, for Gaussian illumination, Eq. (4) is used to generate all the amplitude values in the matrix. A pseudorandom number generator is used to generate uniformly distributed phase values over the interval [0-2π], which acts as a phase random screen. The wave propagation algorithm used is the Direct Method (DM), see [18, 22-24] for details. After speckle intensity images have been numerically generated in the observation planes, two intensity values at $R = (x, 0, z_0)$ and $R' = (x + \gamma, 0, z_0 + \varepsilon)$ are extracted. Running the pseudorandom number generator again, we repeat the recording process until a large number of intensity values at the same positions are obtained. The two sets of values for R and R' respectively make up two vectors, and these are correlated using the Matlab in-built function "normxcorr2" [18, 25] to get the desired correlation coefficient between the two points.

3.2 Simulation results

The speckle correlation function Eq. (5) indicates that the speckle fields in the space will decorrelate in 3D, and more detailed discussions can be found in [18, 19]. Here we provide the simulation results for two of the important directions: the lateral decorrelation between two longitudinally displaced speckle patterns and the on-axis and off-axis longitudinal decorrelation between a series longitudinally displaced speckle patterns.

First we examine the lateral decorrelation. The parameter values used in the simulations are: The matrix dimension $N = 1000$; the sample period in the object plane $\Delta\xi = 21.38$ μm; illuminating spot diameter at the object $2w = 3$ mm; recording distance $z_0 = 400$ mm and $\lambda = 633$ nm. $x = x_1$ is chosen to 3.55 mm. The number of values in each vector is chosen to 1024. The generated speckle patterns in $z = z_0$ and $z = z_0 + \varepsilon$ plane have different sample intervals when the DM is used to simulate the wave propagation, as in Ref. [18], a resizing operation is carried out to maintain the sample interval of the speckle patterns. The simulation results are presented in Fig. 3.

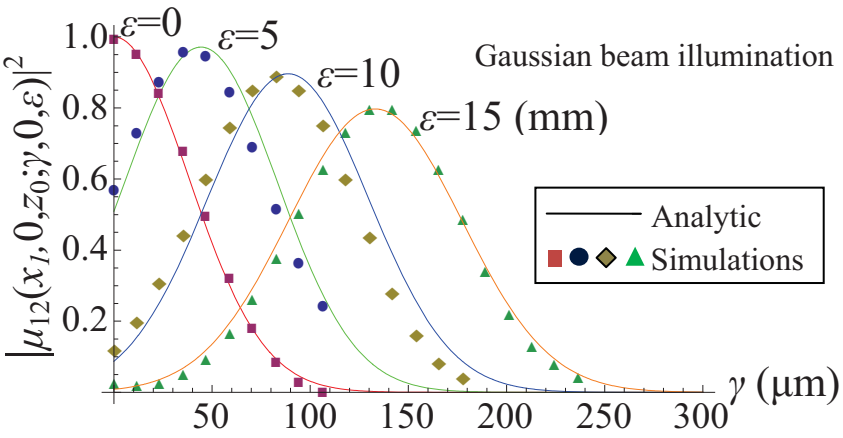

Figure 3. Lateral speckle correlation coefficients between an off-axis field at position $Q_1 = (x_1,0\ z_0)$ in $z = z_0$ plane and fields in a longitudinally displaced plane $z = z_0 + \varepsilon$ (mm), as a function of γ.

We now examine the longitudinal decorrelation. The parameter values are identical with the lateral case, except $\Delta\xi = 10.69$ μm and $z_0 = 200$ mm. Results for four positions, including $x = 0$ (on-axis) and $x = \{1.184, 2.368, 3.552$ mm$\}$ (off-axis), are simulated. Resizing operations to the longitudinally dispalced speckle patterns to maintian the sample interval are also carried out in this simulation. The results are shown in Fig. 4.

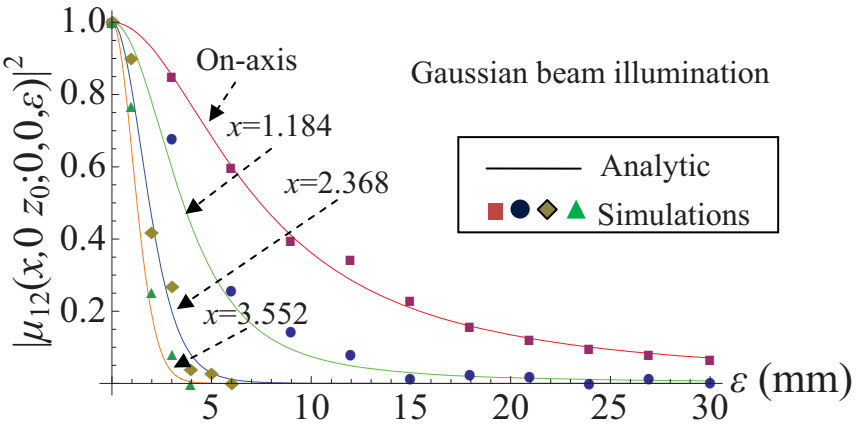

Figure 4. Longitudinal speckle correlation coefficients between field at $Q = (x, 0, z_0)$ in $z = z_0$ plane and a longitudinally displaced field in plane $z = z_0 + \varepsilon$, as a function of ε. x in units of mm.

Comparing the simulating results using time averaging presented here to the results using spatial averaging presented in [18], we find they are very similar, demonstrating that we can interchange the two methods to the calculation of the ensemble average of static speckles. Some differences can be seen between the numerically calculated correlation coefficients and the analytic predictions both here and in [18]. However, the decorrelation trends of the speckle correlation function are quite well simulated, as are the positions of the peak correlation values in the lateral decorrelation. Therefore we do not believe the relatively small absolute disagreements between the numerical results and the analytic predictions are of great practical significance.

4. EXPERIMENTAL VERIFICATION AND APPLICATIONS

In this section we measure the first order statistics of the speckle pattern captured by camera. Through comparison with the prediction of Eq. (11), the effect of camera pixel integration on the statistics of speckle field is experimentally verified.

We also present the measured speckle correlation coefficients to verify the analytic correlation function. As mentioned before, the correlation function is derived based on several critical assumptions. As a result, the verification of the correlation function will provide validity of these assumptions in the physical model for fully developed speckle. Since, the realization of temporally ergodic speckle intensities experimentally is time-consuming, here we generate our results using the spatial averaging.

The experimental system we use depicted in Fig. 1. A Gaussian beam from a Helium-Neon laser of wavelength λ = 633 nm is used as the light source. It is spatially filtered and then collimated by a lens of focal length f = 10 cm. An optical diffuser (100 mm diameter 120 Grit Ground Glass Diffuser) is used at the object plane and the illuminating spot on this object is measured to have a diameter of $2w$ = 8.8 mm. The speckle image is recorded using a CCD camera positioned in the observation plane that is perpendicular to the optical axis. The CCD is mounted on a translation stage (NewPort UTS50PP linear stage having a positional accuracy of ±0.1 μm) so that the longitudinal position of the CCD can be controlled. The CCD used is an 8 bit 4 megapxiel IMPERX IPX-4M15-G, which has 2048×2048 pixels each of size 7.4 μm.

4.1 First order statistics of the captured speckle intensities

Three speckle patterns are captured respectively in planes z_0 = 80 mm, 250 mm and 400 mm. The intensity values of the central row are extracted and used to generate the histogram in order to examine the statistics of the speckle intensities. The height of the histogram is presented in terms of probability density, so that it can be used to compare with the theoretical prediction of Eq. (11), as shown in fig. 5.

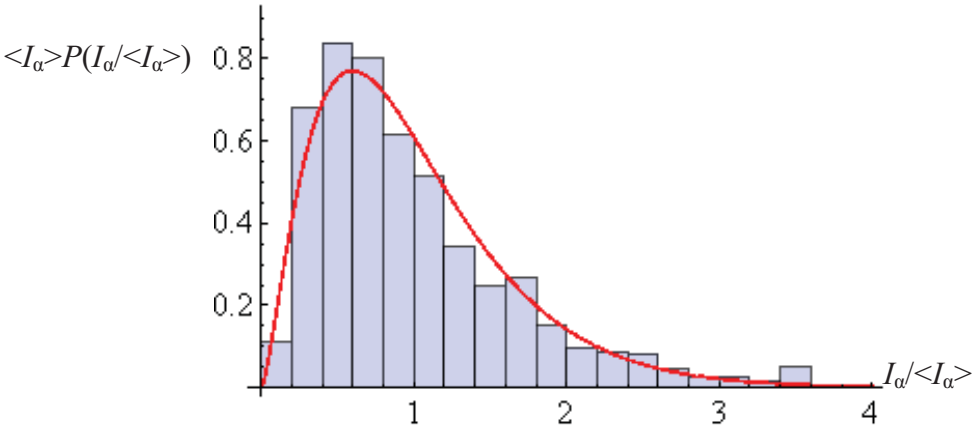

(a)

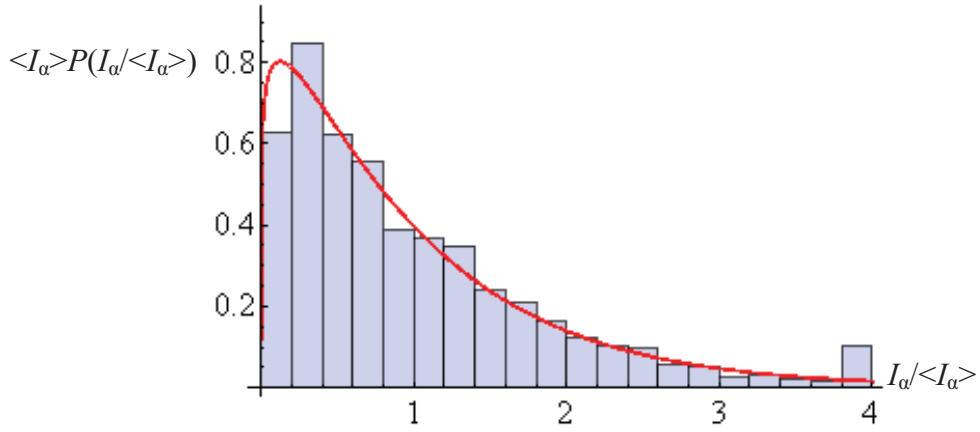

(b)

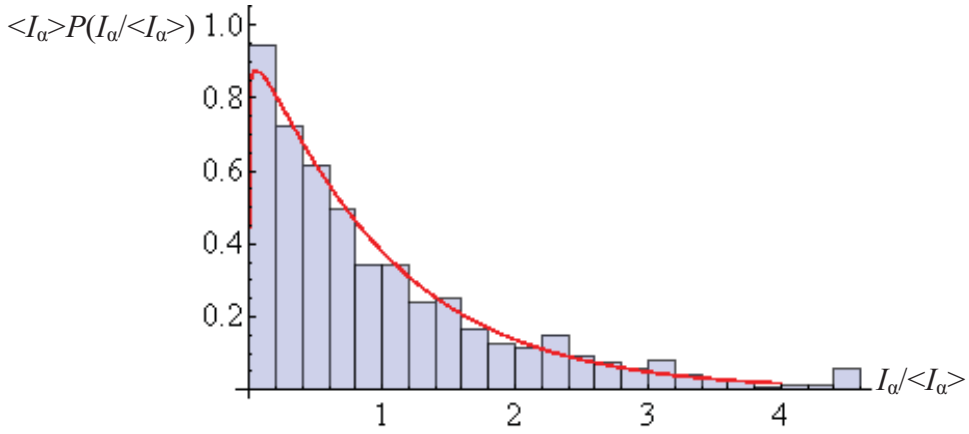

(c)

Figure 5. First order statistics of the captured speckle intensities. The histograms are generated using 2048 intensity values. The solid red curves: PDFs of the intensity values predicted by Eq. (11). (a) For speckle pattern captured at z = 80 mm, in this case, A_D/A_C = 2.020 and M_{au} =2.4975; (b) For speckle pattern captured at z = 250 mm, in this case, A_D/A_C = 0.6464 and M_{au} = 1.1420; (c) For speckle pattern captured at z = 400 mm, in this case, A_D/A_C = 0.4040 and M_{au} = 1.0548.

From Fig. 5, we see that for different A_D/A_C ratios, the PDF of the captured intensities varies, and it is well approximated by the Gamma function described by Eq. (11). The pixel integration effect is to transform the ideal fully developed speckle, whose PDF follows a negative exponential distribution, into a modified PDF having a Gamma distribution. Importantly, this effect can be minimized experimentally by controlling A_D/A_C. As shown in Fig. 5(b) and 5(c), by properly controlling the ratio A_D/A_C, the PDF of the captured speckle intensity can be reduced to the negative exponential distribution of fully developed speckle and thus made to behave as if it were captured by ideal point-like camera.

We note that in each of the experimental results presented in Fig. 5, there is a significant peak for the last histogram "bin". We attribute this effect to a slight saturation of the camera, which was not noticed during the experiment. The reason for this is that there is a slight and artificial increase in the number of intensity values of 255 due to the limitied dynamic range of the 8-bit camera.

4.2 Experimental results for lateral and longitudinal speckle correlation

To study the lateral decorrelation trends, three speckle patterns are captured at the $z = z_0 + \varepsilon$ planes ($z_0 = 250$ mm and $\varepsilon =$ 0, 0.5, and 1 mm). Subset images of size 200×200 pixels are selected from these patterns and correlated using "normxcorr2" [18, 25]. The spatial position for all these subset images' center is $Q_1 = (x_1, 0) = (4.44$ mm, $0)$. Experimental results are shown in Fig. 6, where γ is given in terms of a number of pixels.

In order to compare the experimental results to the analytic continuous correlation function (Eq. (5)), the discrete correlation coefficients obtained from experiment are interpolated. Fig. 6 is generated using a cubic spline interpolation algorithm [26]. As can be seen, the interpolated experimental curves match the theoretical predictions reasonably well.

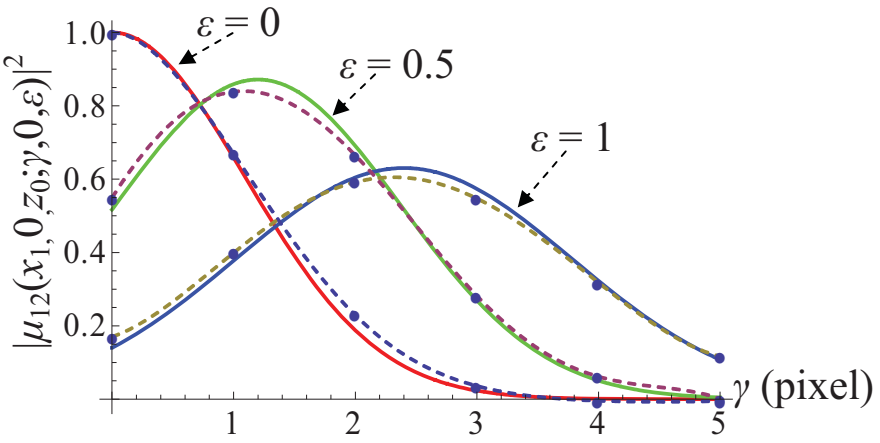

Figure 6. Lateral speckle correlation function for an off-axis field at $Q_1 = (x_1, 0)$ versus lateral shifting γ when $\varepsilon = 0$ mm, $\varepsilon = 0.5$ mm, $\varepsilon = 1$ mm. Dots: Discrete correlation coefficients from experiment. Dashed curve: Cubic spline interpolation based on the experimental data. Solid curve: Theoretical continuous speckle correlation.

For the longitudinal decorrelation trends, ten speckle patterns are captured at the $z = z_0 + \varepsilon$ planes ($z_0 = 250$ mm and $0 \le \varepsilon \le 1.8$ mm, in steps of 0.2 mm). Correlation coefficients for four positions, i.e., $Q = (x, 0) = \{(0, 0)$, (2.22 mm, 0), (4.44 mm, 0), and (6.66 mm, 0)$\}$, were measured, so that the behaviour of both on-axis and off-axis longitudinal correlation coefficients could be examined and compared with the analytic predictions. The results are shown in Fig. 7.

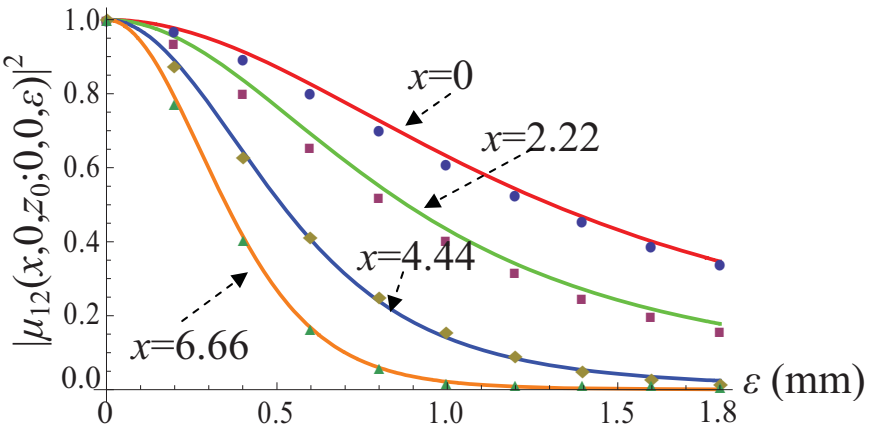

Figure 7. Longitudinal speckle correlation function for an off-axis field at $Q = (x, 0)$ versus longitudinal displacement ε when $x = 0$ mm (on-axis), $x = 2.22$ mm, $x = 4.44$ mm and $x = 6.66$ mm. Dots: Discrete correlation coefficients from experiment. Solid curve: Theoretical continuous speckle correlation.

4.3 Applications

The lateral speckle decorrelation property shown in Fig. 6 indicates that the position of the peak coefficient shifts when a speckle field at off-axis point position is correlated with longitudinally displaced speckle fields. We have found that the shifting value γ is determined by the recording distance z_0, the off-axis observation position x (with respect to the optical axis), and the longitudinal camera displacement ε, see Eq. (12) in [18] and the experiments presented in [19]. By substituting the longitudinal camera displacement ε with the out-of-plane displacement of the object surface, while keeping the camera position steady, this out-of-plane displacement of diffuser surface can be estimated in the observation plane using this lateral decorrelation property. In [19] we have discussed the measurement process in detail, and have shown that the measurement error is approximately one pixel pitch of the camera (7.4 μm) when parameters z_0 and x are reasonably chosen.

The longitudinal speckle decorrelation property shown in Fig. 7 indicates that the off-axis longitudinal speckles decorrelate much faster as the off-axis position moves further away from the system optical axis. This means that when two longitudinally displaced speckle patterns in the observation planes $z = z_0$ and $z = z_0 + \varepsilon$ are correlated, the obtained longitudinal correlation coefficients will monotonically decrease along the radial direction, see [18] and [19] for more detail. Using this property, in [19], we have demonstrated an alignment technique that can be used to locate and align the system optical axis with the camera center. The implementation of this technique and the alignment resolution are discussed in detail in [19] and the final achieved alignment resolution is about 447.7 μm.

5. CONCLUSIONS

The 3D correlation function of static speckles is reviewed and verified using computer simulations and experimental measurements. The pixel integrating effect on speckle correlation coefficients is also analyzed, showing that this effect can be minimized and is negligible once the ratio of the camera pixel size to the correlation extent of speckle pattern is much less than unity. We also show that both time averaging and spatial averaging can be used to realize the ensemble average of the speckle fields. The lateral and longitudinal speckle decorrelation properties are highlighted as their implications for two practical applications: (I) The position shift of the peak coefficient appears when an off-axis speckle field is correlated with the speckle fields in a longitudinally displaced plane, from which the out-of-plane displacement of the diffuser surface can be measured in the observation plane. (II) The longitudinal correlation coefficients of two longitudinally displaced speckle patterns decrease monotonically along the radial direction, based on which an alignment technique to align the system optical axis with the camera centre can be implemented.

ACKNOWLEGDEMENTS

D. Li is supported by a UCD-CSC (University College Dublin - China Scholarship Council) joint scholarship. We also acknowledge the support of the Science Foundation Ireland under the National Development Plan. D. P. Kelly is a Junior-Stiftungs professor of "Optik Design" and is supported by funding from the Carl-Zeiss-Stiftung.

REFERENCES

[1] Leushacke, L. and Kirchner, M., "Three-dimensional correlation coefficient of speckle intensity for rectangular and circular apertures," J. Opt. Soc. Am. **A 7**, 827-832 (1990).
[2] Li, Q. B. and Chiang, F. P., "Three-dimensional dimension of laser speckle," Appl. Opt. **31**, 6287-6291 (1992).
[3] Yoshimura, T. and Iwamoto, S., "Dynamic properties of three-dimensional speckles," J. Opt. Soc. Am. **A 10**, 324-328 (1992).
[4] Yura, H. T., Hanson, S. G., Hansen, R. S. and Rose, B., "Three-dimensional speckle dynamics in paraxial optical systems," J. Opt. Soc. Am. **A 16**, 1402-1412 (1999).
[5] Ward, J. E., Kelly, D. P. and Sheridan, J. T., "Three-dimensional speckle size in generalized optical systems with limiting apertures," J. Opt. Soc. Am. **A 26**, 1885-1864 (2009).
[6] Kelly, D. P., Ward, J. E., Hennelly, B. M., Gopinathan, U., O'Neill, F. T. and Sheridan, J. T., "Paraxial speckle-based metrology system with an aperture," J. Opt. Soc. Am. **A 23**, 2861-2870 (2006).
[7] Kelly, D. P., Ward, J. E., Gopinathan, U., Hennelly, B. M., O'Neill, F. T. and Sheridan, J. T., "Generalized Yamaguchi correlation factor for coherent quadratic phase speckle metrology systems with an aperture," Opt. Lett. **31**, 3444-3446 (2006).
[8] Goodman, J. W., [Speckle Phenomena in Optics: Theory and Applications], 1st ed, Roberts, (2007).
[9] Weigelt, G. P. and Stoffregen, B., "The longitudinal correlation of three-dimensional speckle intensity distribution," Optik (Stuttgart) **48**, 399-408 (1977).
[10] Halford, C. E., Gamble, W. L. and George, N., "Experimental investigation of the longitudinal characteristics of laser speckle," Opt. Eng. **26**, 1263-1264 (1987).
[11] Yamaguchi, I., "Speckle displacement and decorrelation in the diffraction and image fields for small object deformation," Opt. Acta. **28**, 1359-1376 (1981).
[12] Li, D. W. and Chiang, F. P., "Decorrelation functions in laser speckle photography," J. Opt. Soc. Am. **A 3**, 1023-1031 (1986).
[13] Gatti, A., Magatti, D. and Ferri, F., "Three-dimensional coherence of light speckles: Theory," Phys. Rev. A 78, 063806 (2008).
[14] Magatti, D., Gatti, A. and Ferri, F., "Three-dimensional coherence of light speckles: Experiment," Phys. Rev. A 79, 053831 (2009).
[15] Skipetrov, S. E., Peuser, J., Cerbino, R., Zakharov, P., Weber, B. and Scheffold, F., "Noise in laser speckle correlation and imaging techniques," Opt. Express **18**, 14519-14534 (2010).
[16] Goodman, G. W., "Role of coherence concepts in the study of speckle," Proc. Soc. Photo-Opt. Instrum. Eng. **194**, 86-94 (1979).
[17] Naik, D. N., Singh, R. K., Ezawa, T., Miyamoto, Y. and Takeda, M., "Photon correlation holography," Opt. Exp. **19**, 1408-1421 (2011).
[18] Li, D., Kelly, D. P. and Sheridan, J. T., "3D static speckle fields: Part I. Theory and a numerical investigation," accepted for publication in JOSA A, Manuscript ID: 149094, (2011).
[19] Li, D., Kelly, D. P., and Sheridan, J. T., "3D static speckle fields: Part II. Experimental investigation," accepted for publication in JOSA A, Manuscript ID: 149204, (2011).
[20] Kogelnik, H.and Li, T., "Laser beams and resonators," Proc. IEEE **54**, 1312-1329 (1966).
[21] Abramowitz, M. and Stegun, A., [Handbook of Mathematical Functions with Formulas, Graphs, and Mathematical Tables], 9th ed, Dover Publications, (1972)
[22] Mas, D., Garcia, J., Ferreira, C., Bernardo, L. M. and Marinho, F., "Fast algorithms for free-space diffraction patterns calculation," Opt. Comm. 164, 233-245 (1999).
[23] Schnars, U. and Jueptner, W., [Digital Holography: Digital Hologram Recording, Numerical Reconstruction, and Related Techniques], 1st ed, Springer, (2004).

[24] Kelly, D. P., Hennelly, B. M., Rhodes, W. T. and Sheridan, J. T., "Analytical and numerical analysis of linear optical systems," Opt. Eng. 45, 008201-1-008201-12 (2006).
[25] The Mathworks Ins., http://www.mathworks.com/help/toolbox/images/ref/normxcorr2.html, Data retrieved: February 2011.
[26] Wolfram Research Ins, http://reference.wolfram.com/mathematica/ref/Interpolation.html, Data retrieved: February 2011.